J. Fluid Mech. (2007), *vol.* 572, *pp.* 367–387.
doi:10.1017/S0022112006003533 Printed in the United Kingdom

Capillary spreading of a droplet in the partially wetting regime using a diffuse-interface model

By V. V. KHATAVKAR, P. D. ANDERSON† AND H. E. H. MEIJER

Materials Technology, Dutch Polymer Institute, Eindhoven University of Technology, PO Box 513, 5600 MB Eindhoven, The Netherlands

(Received 6 August 2005 and in revised form 17 July 2006)

The spreading of a liquid droplet on a smooth solid surface in the partially wetting regime is studied using a diffuse-interface model based on the Cahn–Hilliard theory. The model is extended to include non-90° contact angles. The diffuse-interface model considers the ambient fluid displaced by the droplet while spreading as a liquid. The governing equations of the model for the axisymmetric case are solved numerically using a finite-spectral-element method. The viscosity of the ambient fluid is found to affect the time scale of spreading, but the general spreading behaviour remains unchanged. The wettability expressed in terms of the equilibrium contact angle is seen to influence the spreading kinetics from the early stages of spreading. The results show agreement with the experimental data reported in the literature.

1. Introduction

The spreading of a liquid droplet on a solid surface under capillary action, referred to as spontaneous spreading, plays an important role in diverse technologies such as the application of paints, inkjet printing, adhesives and insecticides, migration of inks on paper, catalysis, oil recovery, etc. The droplet spreads by displacing another immiscible fluid (the ambient fluid), which is usually air but may also be a liquid. The spreading may be characterized, according to whether the equilibrium contact angle is zero or finite, as being complete or partial wetting. The spreading kinetics in the complete wetting regime has been extensively studied and covered in several reviews and references therein; see for example Dussan V. (1979), Marmur (1983), de Gennes (1985), Blake (1993) and Kistler (1993). In this case, it has been shown that at large times the radius of the contact area of the droplet with a solid surface follows $r \propto t^{1/7}$ if the dissipation in the vicinity of the contact line dominates and $r \propto t^{1/10}$ if the viscous loss inside the droplet dominates. In contrast, only a few studies have explored the partially wetting regime (Foister 1990; de Gennes, Hua & Levinson 1990; Zosel 1993; Seaver & Berg 1994; de Ruijter, Coninck & Oshanin 1999; de Ruijter *et al.* 2000). Theoretical approaches developed by de Gennes *et al.* (1990), Seaver & Berg (1994) and de Ruijter *et al.* (1999, 2000) provide useful insight although they use some simplifying assumptions with regard to flow (such as the lubrication approximation) and the shape of the droplet in order to yield an analytically tractable model. In general the assumptions made are only valid for very small equilibrium contact angles. So, when the equilibrium contact angle is large, e.g. $\theta \approx 90°$, a detailed

† Author to whom correspondence should be addressed: p.d.anderson@tue.nl

model with a possible numerical implementation may, in general, be required. The model applied should address the following issues:

(i) tracking of the droplet–ambient-fluid interface and accounting for the surface tension;

(ii) resolving the contact-line singularity;

(iii) incorporating the effects of substrate wettability.

Rather than a classical sharp-interface model we will use a diffuse-interface model and it is our aim to determine how droplet spreading in the partially wetting regime compares with the experiments reported in the literature.

The diffuse-interface model (DIM) is based on the idea that the fluid–fluid interface has a finite thickness over which various thermodynamic variables change continuously. The concept was first used by van der Waals (1893) to explain why equilibrium interfaces have surface tension and, hence, DIM is endowed with capillarity. The thickness of the interface is closely related to the finite range of molecular interactions (Rowlinson & Widom 1989). The finite-interaction range is represented by a non-local effect in the free energy: the local free-energy density depends not only on the local composition but also on the composition of the immediate environment (Davis & Scriven 1982). By using a mean-field approximation, the non-local effect in the free energy is represented by a dependence on the local composition gradients rather than on the non-local composition (Cahn & Hilliard 1958). This free energy determines both the interfacial thickness and the surface tension that now appears (after coupling with the equations of motion) as a distributed stress over the interfacial region. The position and the shape of the interface is a part of the solution – which is continuous throughout the system but may have large variations in the interfacial region – of the governing equations of DIM.

Originally designed to model the initial stages of spinodal decomposition by Cahn (1965), the diffuse-interface approach has been used to model a wide range of hydrodyanmic and interfacial phenomena, for example, mixing (Chella & Viñals 1996; Keestra *et al.* 2003), topological transitions, i.e. the breakup and coalescence of drops (Lowengrub & Truskinovsky 1998; Jacqmin 1999; Verschueren 1999; Lee, Lowengrub & Goodman 2002*a*, *b*), contact-line dynamics (Seppecher 1996; Chen, Jasnow & Viñals 2000; Jacqmin 2000), thermocapillary flow (Jasnow & Viñals 1996; Verschueren, van de Vosse & Meijer 2001) and two-phase flows of complex fluids (Yue *et al.* 2004). For more details see the reviews by Anderson, McFadden & Wheeler (1998) and Naumann & He (2001). The diffuse-interface model could be extended to incorporate non-90° contact angles (in § 2.2 it is shown that the 90° contact angle appears 'naturally' in the model) and, following Cahn (1977) and Jacqmin (2000), this has been achieved by postulating that the wall free energy, which captures the wall–fluid interactions, depends only on the composition at the wall.

The resolution of the contact, line singularity in a diffuse-interface model, which occurs in spite of the application of a strict no-slip boundary condition, is by chemical-potential-gradient-induced diffusion; see the analyses perfomed by Seppecher (1996), Chen *et al.* (2000), Jacqmin (2000) and, more recently, Briant, Wagner & Yeomans (2004) and Briant & Yeomans (2004). A similar approach, modelling the moving contact line with an interface of finite thickness, has been developed by Shikhmurzaev (1993*a*, *b*, 1994, 1997*a*, *b*). His approach differs from the one presented here in that the interface between the two bulk phases is considered as a third 'surface' phase having its own viscosity, density and equation of state.

In this paper, we use the Cahn–Hilliard diffuse-interface approach to model the spreading of a liquid droplet on a perfectly smooth chemically homogeneous solid

surface. This is done in order to compare diffuse-interface spreading behaviour in a partially wetting regime with the experiments of Foister (1990) and Zosel (1993). The model applied is a two-phase model and, hence, the effect of the ambient-fluid viscosity on the spreading behaviour is investigated. The wettability of the solid surface, which may affect the spreading kinetics, is also studied by varying the equilibrium contact angle over a wide range from 20° to 120°.

The paper is organized as follows. In the next section the diffuse-interface model, which accounts for partial wetting, is briefly reviewed. Section 3 gives the system definition to which the model is applied. The numerical method used to solve the equations is described briefly in § 4. Results are presented and discussed in § 5. Finally, § 6 contains some conclusions.

2. Model equations

The diffuse-interface model used (for details see Lowengrub & Truskinovsky 1998; Verschueren 1999) is a two-phase model applied to a fluid consisting of two partially miscible components. The fluid, referred to as a binary fluid, is assumed to have a specific Helmholtz free energy f, based on the work of Cahn & Hilliard (1958), which reads

$$f(c, \nabla c) = f_0(c) + \tfrac{1}{2}\epsilon|\nabla c|^2, \tag{2.1}$$

where c is the mass fraction of one of the components, f_0 is the homogeneous part of the specific free energy and ϵ is the gradient energy parameter. The homogeneous part f_0 is here most simply given by the so-called c^4 approximation (Gunton, Miguel & Sahni 1983), also known as the Ginzburg–Landau free energy:

$$f_0(c) = \tfrac{1}{4}\beta c^4 - \tfrac{1}{2}\alpha c^2, \tag{2.2}$$

where α and β are both positive constants for an isothermal system below its critical temperature. Combining (2.1) and (2.2), f can now be written as

$$f = \tfrac{1}{4}\beta c^4 - \tfrac{1}{2}\alpha c^2 + \tfrac{1}{2}\epsilon|\nabla c|^2. \tag{2.3}$$

The chemical potential is defined as the variational derivative of the specific Helmholtz free energy (2.3) with respect to concentration:

$$\mu = \frac{\delta f}{\delta c} = \beta c^3 - \alpha c - \epsilon\nabla^2 c. \tag{2.4}$$

For a planar interface (with z as the direction normal to the interface) at equilibrium ($\mu = 0$ in (2.4)) the corresponding concentration profile is given by

$$c(z) = c_B \tanh\left(\frac{z}{\sqrt{2}\xi}\right), \tag{2.5}$$

where $c_B = \pm\sqrt{\alpha/\beta}$ are the equilibrium bulk concentrations (for example, $c_B = \sqrt{\alpha/\beta}$ corresponds to the droplet and $c_B = -\sqrt{\alpha/\beta}$ corresponds to the ambient fluid) and $\xi = \sqrt{\epsilon/\alpha}$ is the interface thickness.

The interfacial tension γ_{lv} is the excess free energy per unit surface area due to the inhomogeneity in c in the interfacial region (Rowlinson & Widom 1989)

$$\gamma_{lv} = \epsilon\int_{-\infty}^{\infty}\left(\frac{\mathrm{d}c}{\mathrm{d}z}\right)^2 \mathrm{d}z. \tag{2.6}$$

Using the equilibrium concentration profile yields

$$\gamma_{lv} = \frac{2\sqrt{2}}{3}\frac{\epsilon c_B^2}{\xi}. \tag{2.7}$$

For the mass conservation of individual components, the mass fraction c satisfies the local balance equation:

$$\frac{\partial c}{\partial t} + \boldsymbol{v}\cdot\nabla c = \nabla\cdot M\nabla\mu, \tag{2.8}$$

where M is the mobility, which, in general, can be a function of c. In the above equation, known as the Cahn–Hilliard equation, the diffusional flux is assumed to be proportional to the gradient of the chemical potential. This equation was originally used to describe the initial stages of spinodal decomposition (Cahn 1965).

The governing equations for flow are obtained by coupling the momentum and total mass balance with the DIM equations, which yields a modified Navier–Stokes equation (Lowengrub & Truskinovsky 1998; Verschueren 1999):

$$\rho\left(\frac{\partial \boldsymbol{v}}{\partial t} + (\boldsymbol{v}\cdot\nabla\boldsymbol{v})\right) = -\nabla p + \nabla\cdot\eta\left[(\nabla\boldsymbol{v}) + (\nabla\boldsymbol{v})^T\right] + \rho(\mu\nabla c - \nabla f) + \rho\boldsymbol{g}, \tag{2.9}$$

where p is the pressure, $\boldsymbol{v}$ is the barycentric velocity and $\boldsymbol{g}$ is the gravitational force per unit mass. The viscosity η is assumed to have the following linear relationship with the concentration c:

$$\eta = \eta_d\left(\frac{c+1}{2}\right) - \eta_c\left(\frac{c-1}{2}\right), \tag{2.10}$$

where η_d and η_c are the viscosities of the droplet and ambient fluid respectively. The density of the binary fluid ρ can be considered as a function of the concentration c, to account for the different densities of the two phases, for example using the simple mixture rule (Joseph & Renardy 1993)

$$\frac{1}{\rho} = \frac{1}{\rho_d}\left(\frac{c+1}{2}\right) - \frac{1}{\rho_c}\left(\frac{c-1}{2}\right), \tag{2.11}$$

where ρ_d and ρ_c are the density of the droplet and of the ambient fluid, respectively. The equation of continuity which takes quasi-incompressibility (Lowengrub & Truskinovsky 1998) into account is

$$\nabla\cdot\rho\boldsymbol{v} = 0. \tag{2.12}$$

Note that an equation similar to (2.8) can be written for the other component of the binary fluid. However, for the present binary case we choose to work with the one-component mass-balance equation (2.8) and the total mass-balance equation (2.12).

2.1. *Non-dimensionalized governing equations*

The governing equations are non-dimensionalized using the following dimensionless variables:

$$c^* = \frac{c}{c_B}, \quad \nabla^* = L\nabla, \quad \mu^* = \frac{\mu\xi^2}{\epsilon c_B}, \quad f^* = \frac{f\xi^2}{\epsilon c_B^2}, \quad \boldsymbol{v}^* = \frac{\boldsymbol{v}}{V},$$
$$t^* = \frac{tV}{L}, \quad p^* = \frac{pL}{\eta_d V}, \quad \boldsymbol{g}^* = \frac{\boldsymbol{g}}{g}, \quad \eta^* = \frac{\eta}{\eta_d}, \quad \rho^* = \frac{\rho}{\rho_d}.$$

The characteristic length and velocity scales (as yet undefined) are denoted by L and V, respectively. The acceleration due to gravity is represented by g.

The system of equations reads, after dropping the asterisks,

$$\frac{\partial c}{\partial t} + \boldsymbol{v}\cdot\nabla c = \frac{1}{Pe}\nabla^2\mu, \tag{2.13}$$

$$\mu = c^3 - c - C_h^2\nabla^2 c, \tag{2.14}$$

$$f = \tfrac{1}{4}c^4 - \tfrac{1}{2}c^2 + \tfrac{1}{2}C_h^2|\nabla c|^2, \tag{2.15}$$

$$Re\,\rho\left(\frac{\partial \boldsymbol{v}}{\partial t} + \boldsymbol{v}\cdot\nabla\boldsymbol{v}\right) = -\nabla p + \nabla\cdot\eta\left[(\nabla\boldsymbol{v}) + (\nabla\boldsymbol{v})^T\right] + \frac{1}{CaC_h}\rho(\mu\nabla c - \nabla f) + \frac{Bo}{Ca}\rho\boldsymbol{g}, \tag{2.16}$$

$$\eta = \left(\frac{c+1}{2}\right) - \frac{1}{\lambda}\left(\frac{c-1}{2}\right). \tag{2.17}$$

$$\frac{1}{\rho} = \left(\frac{c+1}{2}\right) - \kappa\left(\frac{c-1}{2}\right), \tag{2.18}$$

$$\nabla\cdot\rho\boldsymbol{v} = 0, \tag{2.19}$$

The dimensionless groups that appear are the Péclet number Pe, the Cahn number C_h, the Reynolds number Re, the capillary number Ca, the Weber number We, the Bond number Bo, the density ratio κ and the viscosity ratio λ, and they are defined as follows:

$$Pe = \frac{VL\xi^2}{M\epsilon}, \quad C_h = \frac{\xi}{L}, \quad Re = \frac{\rho_d V L}{\eta_d}, \quad Ca = \frac{\eta_d V}{\gamma_{lv}},$$
$$We = \frac{\rho_d V^2 L}{\gamma_{lv}} = Re\ Ca, \quad Bo = \frac{\rho_d L^2 \mathrm{g}}{\gamma_{lv}}, \quad \kappa = \frac{\rho_d}{\rho_c}, \quad \lambda = \frac{\eta_d}{\eta_c}.$$

2.2. *Partial-wetting boundary conditions*

The wall for e.g. the solid surface at $z = 0$ may be preferentially wetted by one component of the binary fluid. This effect may be accounted for by approach given in Cahn (1977), where solid–fluid interactions are assumed to be short-range. According to this assumption, the total system free energy $\mathscr{F}$ can be written as

$$\mathscr{F} = \int_\Omega f\,\mathrm{d}\Omega + \int_\Gamma f_w\,\mathrm{d}\Gamma, \tag{2.20}$$

where f_w is the specific wall free energy, which depends only on the concentration at the wall, and Ω is the domain volume bounded by the surface Γ. The surface-integral term in the above equation represents the contribution of solid–fluid interactions.

At equilibrium $\mathscr{F}$ is at its minimum. Minimizing $\mathscr{F}$, using methods of variational calculus subject to a natural boundary condition (Beveridge & Schechter 1970), gives the following boundary condition on the surface Γ:

$$-\epsilon\frac{\partial c}{\partial n_b} + \frac{\partial f_w}{\partial c} = 0, \tag{2.21}$$

where n_b is the direction normal to the boundary.

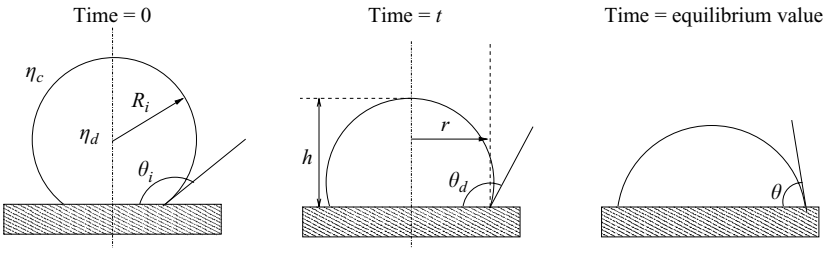

FIGURE 1. Schematic representation of the spreading of a drop on a solid surface.

For f_w we use the form proposed by Jacqmin (2000), which reads

$$f_w = \phi\left(c - \frac{c^3}{3}\right), \tag{2.22}$$

where ϕ is assumed to be constant and is referred to as the wetting potential; but in a more general case, where the solid surface may be chemically heterogeneous, it can be a function of spatial coordinates. With f_w of the form (2.22), $\partial f_w/\partial c$ evaluated at c_B is zero, so at equilibrium no wall layer exists.

Equations (2.21) and (2.22) are non-dimensionalized using the dimensionless variables defined in § 2.1, with the addition of γ_{lv} as the characteristic scale for the specific wall free energy, to give

$$-C_h\frac{\partial c}{\partial n_b} + \Phi(1-c^2) = 0, \tag{2.23}$$

$$f_w = \Phi\left(c - \frac{c^3}{3}\right), \tag{2.24}$$

where $\Phi = \frac{\phi c_B}{\gamma_{lv}}$ is the dimensionless wetting potential.

Using Young's equation, which connects the contact angle with the surface and interfacial tensions of the liquid (γ_{lv}) and the solid (γ_{sv}, γ_{sl}),

$$\cos\theta = \frac{\gamma_{sv} - \gamma_{sl}}{\gamma_{lv}}, \tag{2.25}$$

Φ can be related to the (equilibrium) contact angle θ with the result:

$$\cos\theta = \tfrac{4}{3}\Phi. \tag{2.26}$$

From (2.26) it may be concluded that for a contact angle θ equal to 90°, Φ is zero and the mixed boundary condition (2.23) reduces to a natural boundary condition.

3. System definition

The model described in the previous section is quite general and can be used to analyse spreading of droplets ranging from centimetre to micrometre size. Here, we consider the spreading of a micrometre-size liquid droplet on a smooth chemically homogeneous solid surface, as shown in figure 1. The initial droplet shape is that of a spherical cap, so the problem can be described using axisymmetric coordinates. The droplet spreads by displacing the ambient fluid, which may be an inviscid gas or a viscous liquid. Hence, in general, the flow of the ambient fluid may affect the spreading process and cannot be neglected. The DIM applied in this paper considers this general case. Since small droplets, of about tens of micrometres in diameter, and low spreading rates, typically a few mm s^{-1}, are being considered, typical values of

We, *Re* and *Bo*, using the initial droplet diameter as a characteristic length scale, are 1×10^{-4}, 0.1 and 1×10^{-3}, respectively. Therefore the gravitational and inertial forces, although the flow is inherently unsteady, are assumed to be negligible. It should be mentioned that the experiments of Foister (1990) and Zosel (1993), with which our results will be compared, were performed under similar conditions. Owing to these considerations, the density difference between the droplet liquid and the ambient fluid does not play a significant role and hence the densities are assumed to be equal.

Note that, owing to the particular choice of characteristic velocity scale, γ_{lv}/η_d, used here, the capillary number is equal to unity. Also, the choice of the initial droplet diameter as a characteristic length scale is not unique and another scale such as the interface thickness could be used. However, as the focus here is on the overall spreading behaviour rather than on some phenomenon occurring over the interfacial region, we use the initial droplet diameter. This introduces a small parameter C_h into the problem. In fact, proper scaling is still an open issue in the diffuse-interface model; see for example Lowengrub & Truskinovsky (1998) and Verschueren (1999). Under the above assumptions and using u and v to denote the radial and axial component of the velocity, respectively, the non-dimensional governing equations (2.13)–(2.19) take the following form:

$$\frac{\partial c}{\partial t} + u\frac{\partial c}{\partial r} + v\frac{\partial c}{\partial z} = \frac{1}{Pe}\left[\frac{1}{r}\frac{\partial}{\partial r}\left(r\left(\frac{\partial \mu}{\partial r}\right)\right) + \frac{\partial}{\partial z}\left(\frac{\partial \mu}{\partial z}\right)\right], \tag{3.1}$$

$$\mu = c^3 - c - C_h^2\left[\frac{1}{r}\frac{\partial}{\partial r}\left(r\frac{\partial c}{\partial r}\right) + \frac{\partial^2 c}{\partial z^2}\right], \tag{3.2}$$

$$f = \frac{c^4}{4} - \frac{c^2}{2} + C_h^2\left[\left(\frac{\partial c}{\partial r}\right)\left(\frac{\partial c}{\partial r}\right) + \left(\frac{\partial c}{\partial z}\right)\left(\frac{\partial c}{\partial z}\right)\right], \tag{3.3}$$

$$0 = -\frac{\partial p}{\partial r} + \left[\frac{1}{r}\frac{\partial}{\partial r}\left(r\left(2\eta\frac{\partial u}{\partial r}\right)\right) - \frac{2\eta u}{r^2} + \frac{\partial}{\partial z}\left(\eta\left(\frac{\partial u}{\partial z} + \frac{\partial v}{\partial r}\right)\right)\right] + \frac{1}{C_h}\left(\mu\frac{\partial c}{\partial r} - \frac{\partial f}{\partial r}\right), \tag{3.4}$$

$$0 = -\frac{\partial p}{\partial z} + \left[\frac{1}{r}\frac{\partial}{\partial r}\left(r\left(\eta\left(\frac{\partial u}{\partial z} + \frac{\partial v}{\partial r}\right)\right)\right) + \frac{\partial}{\partial z}\left(2\eta\left(\frac{\partial v}{\partial z}\right)\right)\right] + \frac{1}{C_h}\left(\mu\frac{\partial c}{\partial z} - \frac{\partial f}{\partial z}\right), \tag{3.5}$$

$$\frac{1}{r}\frac{\partial (ru)}{\partial r} + \frac{\partial v}{\partial z} = 0. \tag{3.6}$$

3.1. *Flow boundary conditions at the solid surface*

From the analysis of Huh & Scriven (1971) it is known that application of a no-slip boundary condition for a moving contact line using a classical sharp-interface approach leads to a stress singularity. In fact, the existence of partial slip, which alleviates this problem, has been confirmed by several molecular-dynamics simulations (Koplik, Banavar & Willemsen 1988, 1989; Thompson & Robbins 1989, 1990; Barrat & Bocquet 1999). The nature of slip, though, is complex and has been shown to be related to the microscale fluid physics in the vicinity of the solid (Cieplak, Koplik & Banavar 2001). Slip can be considered either as shear-induced (Dussan V. & Davis 1974; Hocking 1977; de Gennes 1985; Durbin 1988) or as attributable to

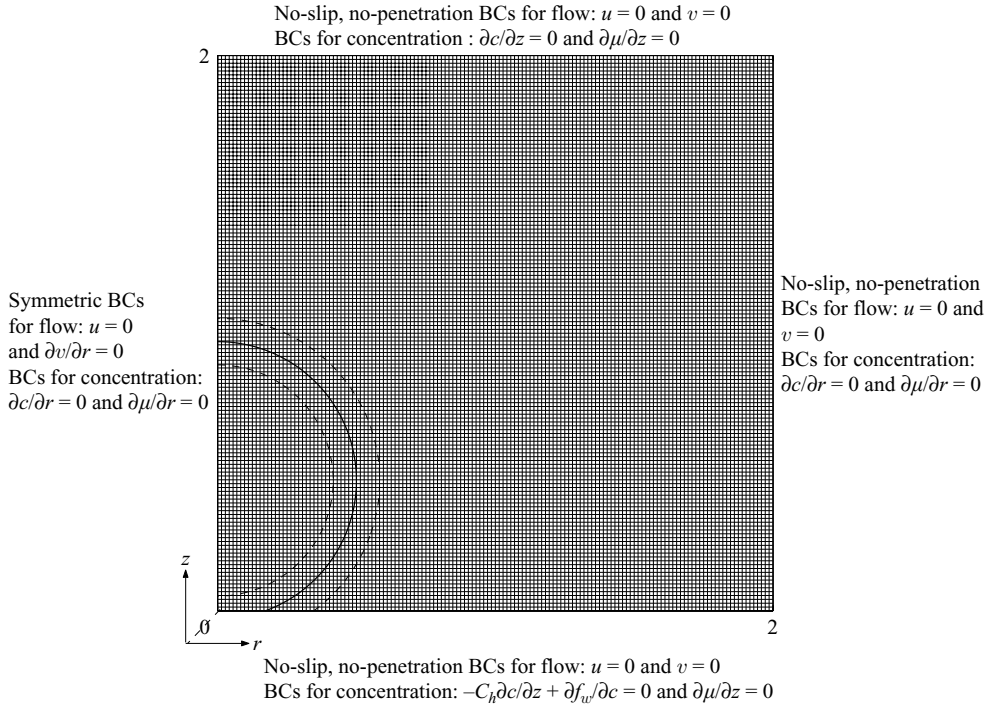

FIGURE 2. The computational domain, mesh, initial and boundary conditions used for the droplet-spreading simulations. The dashed lines represent $c = \pm 0.9$ contours. BC, boundary condition.

fluid–wall interactions (Barrat & Bocquet 1999; Cieplak *et al.* 2001). In the diffuse-interface model, the contact line moves via diffusion driven by the gradients of the chemical potential; these account for fluid–wall interactions, as shown by Seppecher (1996), Chen *et al.* (2000) and Jacqmin (2000). Jacqmin (2000) also showed that regularization of the moving contact line through shear-induced slip and regularization via chemical diffusion give the same macroscopic behaviour. Hence, we apply a no-slip no-penetration flow boundary condition at the solid surface:

$$\boldsymbol{v} = \boldsymbol{0}. \tag{3.7}$$

To specify the contact angle we apply boundary condition (2.23) assuming that the wall at $z = 0$ is at local equilibrium. Other boundary conditions that are applied are (as shown in figure 2) a no-mass-flux condition for the chemical potential,

$$\nabla \mu \cdot \boldsymbol{n} = 0, \tag{3.8}$$

where $\boldsymbol{n}$ is the unit normal vector to the boundary, and a symmetry boundary condition on the left-hand boundary.

4. Numerical method

The flow problem (3.3)–(3.6) is solved in primitive variables, i.e. in a velocity–pressure formulation, and discretized by a standard Galerkin finite-element method (GFEM). Taylor–Hood quadrilateral elements, with continuous pressure, which

employ a biquadratic approximation for velocity and a bilinear approximation for pressure, are used.

The set of two second-order differential equations (3.1)–(3.2) that constitutes the concentration problem is solved in a coupled way. For the temporal discretization of (3.1), a first-order Euler implicit scheme is employed, and the nonlinear term in (3.2) is linearized by a Picard iteration.

The weak form in the present axisymmetric case is derived following the approaches of Gerritsma & Phillips (2000) and Fournier *et al.* (2004), where the cylindrical radius appearing in the definition of the infinitesimal volume element is incorporated into the weighting function. This is done to circumvent the trivial solution ('0 = 0') that may arise from the application of Gauss–Lobatto–Legendre quadrature to axisymmetric problems. The resulting set of discretized equations written in matrix form reads

$$\begin{bmatrix} \boldsymbol{M} + \Delta t \tilde{\boldsymbol{N}}_c^{n-1} & \dfrac{\Delta t}{Pe}\left(\tilde{\boldsymbol{S}}_\mu - \tilde{\boldsymbol{N}}_{\mu c}\right) \\ \left[1 - \left(c_{i-1}^n\right)^2\right]\boldsymbol{M} + 2\Phi C_h c_{i-1}^n \boldsymbol{M}_{BC} - C_h^2(\tilde{\boldsymbol{S}}_c - \tilde{\boldsymbol{N}}_{c\mu}) & \boldsymbol{M} \end{bmatrix} \begin{bmatrix} c_i^n \\ \mu_i^n \end{bmatrix} = \begin{bmatrix} \boldsymbol{M} c_0^{n-1} \\ \Phi C_h \left[1 + \left(c_{i-1}^n\right)^2\right] \boldsymbol{M}_{BC} \end{bmatrix}, \quad (4.1)$$

where c_i^n is the discretized concentration at the ith Picard iteration at time step n, μ_i^n is the discretized chemical potential at the ith Picard iteration at time step n, c^{n-1} is the discretized concentration at time step $n-1$, Δt is the time-step size, $\boldsymbol{M}$ is the mass matrix, $\tilde{\boldsymbol{N}}_c$ is the convection matrix, $\tilde{\boldsymbol{S}}_\mu$ is the Cartesian diffusion matrix, $\boldsymbol{M}_{BC}$ is the mass matrix arising through the linearization of boundary condition (2.23) and $\tilde{\boldsymbol{S}}_c$ is the Cartesian diffusion matrix; $\tilde{\boldsymbol{N}}_{c\mu}$ and $\tilde{\boldsymbol{N}}_{\mu c}$ are convection-like matrices resulting from the description in axisymmetric coordinates and operating on c and μ, respectively. The discretized set of linear algebraic equations is solved using a direct method based on a sparse multifrontal variant of Gaussian elimination (HSL/MA41) (Amestoy & Duff 1989*a*, *b*; Amestoy & Puglisi 2002).

The scheme to advance in time is as follows.

Step 1. Given the initial concentration profile c_0^0, compute f^0, μ^0 and η.

Step 2. Solve the system for the velocity $\boldsymbol{v}^1$ with the terms containing the concentration treated explicitly.

Step 3. Solve the system (4.1) iteratively for concentration c^1 and chemical potential μ^1. Iterations are required owing to the nonlinear term. Iteration is started with $c_1^1 = c^0$ and stopped when $\max|c_i^1 - c_{i-1}^1| \leqslant \delta_c$. The tolerance δ_c for the Picard iteration is set equal to 10^{-6}.

Step 4. Update the time, compute f^1 and η and repeat steps 2–4.

This numerical scheme is implemented in the finite-element package SEPRAN (Segal 1995) and used for simulating droplet spreading on a computational domain spanning dimensionless length 2 in both the radial and the axial direction, as shown in figure 2. The calculations start at the instant the droplet (actually the droplet–ambient-fluid interface, whose position is given by the contour $c = 0$) has a 160° contact angle with the solid surface. The droplet spreads because the initially prescribed contact angle θ_i is not equal to the equilibrium contact angle θ.

5. Results and discussion

The results obtained for droplet spreading in a partially wetting regime with θ ranging from 20° to 120° are presented mainly as semilogarithmic plots of the

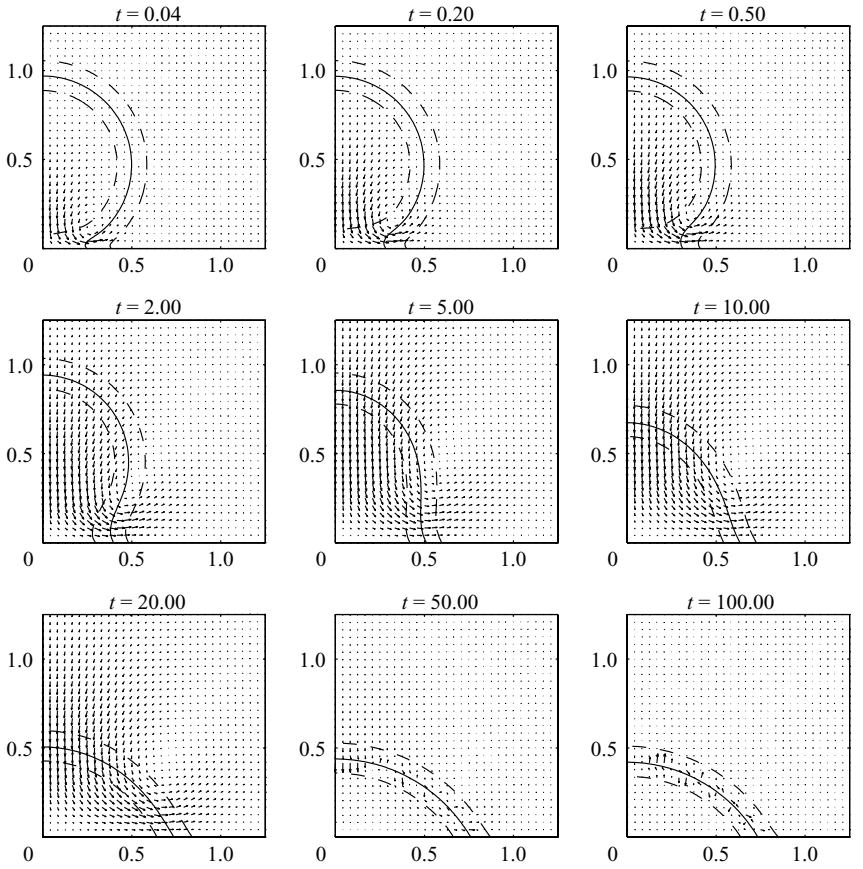

FIGURE 3. Droplet shapes with the corresponding velocity-vector field at different times during spreading, obtained for $C_h = 0.04$, $Pe = 50$, $\lambda = 1$, $\theta = 60^\circ$ and $\Delta t = 10^{-2}$ on a mesh of 90×90 elements. The dashed lines represent $c = \pm 0.9$ contours.

dimensionless radius of the contact circle, r, which is defined as the position where the $c = 0$ contour intersects with the solid surface at $z = 0$, against the dimensionless time t. The time, the radius r and the droplet height h are made dimensionless using the initial droplet radius R_i as a representative length scale.

5.1. *Some general aspects of spreading in the partially wetting regime*

Figure 3 shows droplet shapes (with the corresponding velocity field superimposed as a vector plot) at different times after the start of spreading. Calculations were performed using $C_h = 0.04$, $Pe = 50$, $\lambda = 1$, $\theta = 60^\circ$ and $\Delta t = 10^{-2}$ on a mesh consisting of 90×90 second-order finite spectral elements. This example demonstrates some features found to be common to almost all the spreading calculations reported here. First, the contact angle relaxes locally fast in about $t \approx 0.2$ from the initially prescribed value of 160° to its equilibrium value. During this time, the droplet base (the radius of the contact circle) spreads fast without influencing the global shape of the droplet. This can be rationalized by remembering that at the start of the process the contact-line region is out of equilibrium, i.e. the three surface forces are not balanced, which creates a local gradient of capillary pressure leading to fast initial spreading. At about $t \approx 1$ the droplet apex attains a noticeable downstream velocity

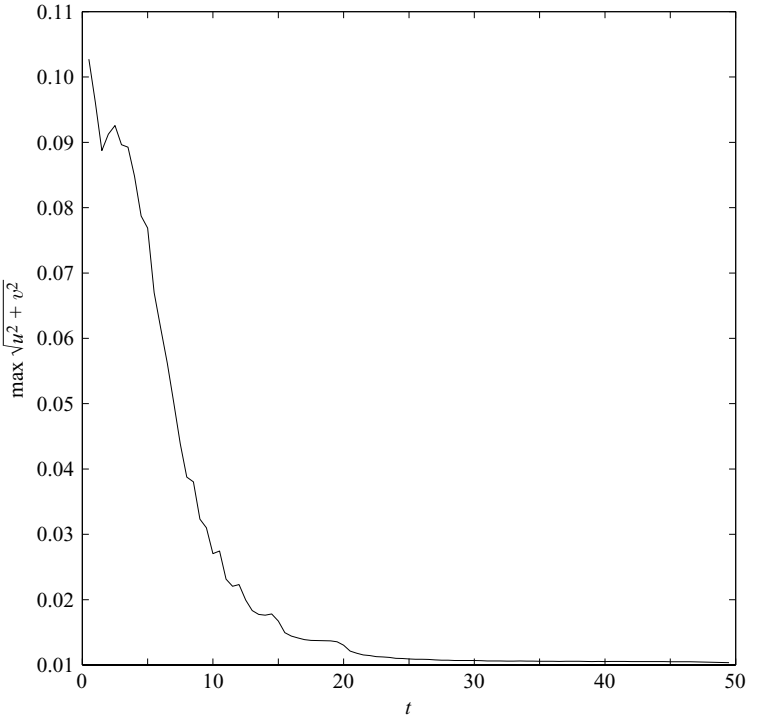

FIGURE 4. The decay in velocity with time for the case shown in figure 3.

and then the global droplet shape begins to change. Then the droplet spreads with continuous changes in its (global) shape until $t \approx 20$. Beyond this time the spreading process progressively slows down and comes to a halt, inferred from the decay in velocity (see figure 4) at about $t \approx 50$. At some points in the interfacial region velocity vectors are still seen to be present, but the magnitude of the velocity is about two orders smaller than that at, say, $t \approx 1$. The droplet might now be expected to remain stationary with a fixed radius of contact with the solid surface. Instead it starts to slowly dissolve into the ambient fluid. This can be recognized more clearly in figure 5 where the droplet profiles corresponding to $t = 50$, 70 and 100 may be compared. This solubility is a result of the partial miscibility of the components of the binary fluid in the c^4 description of the free energy and was roughly shown to be equal to πC_h by Naumann & He (2001) and Keestra *et al.* (2003).

Figure 6 gives semilogarithmic plots of the radius of the contact circle r and the drop height h versus time t, and three stages are indicated. In stage A the radius r increases at almost constant height h. In stage B the droplet spreads with continuous changes in its global shape and r seems to follow $r \propto t^n$, which was reported in the literature for spreading in the complete wetting regime for $t > 100$, with values of n found to be in the range of 0.1 to 0.1428 (for more details see Marmur 1983). Finally, stage C represents the end of the spreading process.

5.2. *Effect of viscosity ratio*

In figure 7 the spreading behaviour obtained for $\lambda = 0.1$, 1, 10 and 100 at an equilibrium contact angle $\theta = 90^\circ$ may be compared. It is apparent that, as expected, the decrease in viscosity of the ambient fluid leads to faster spreading. For t in between 1 to 10 the three curves are almost parallel. Fitting this part of these curves

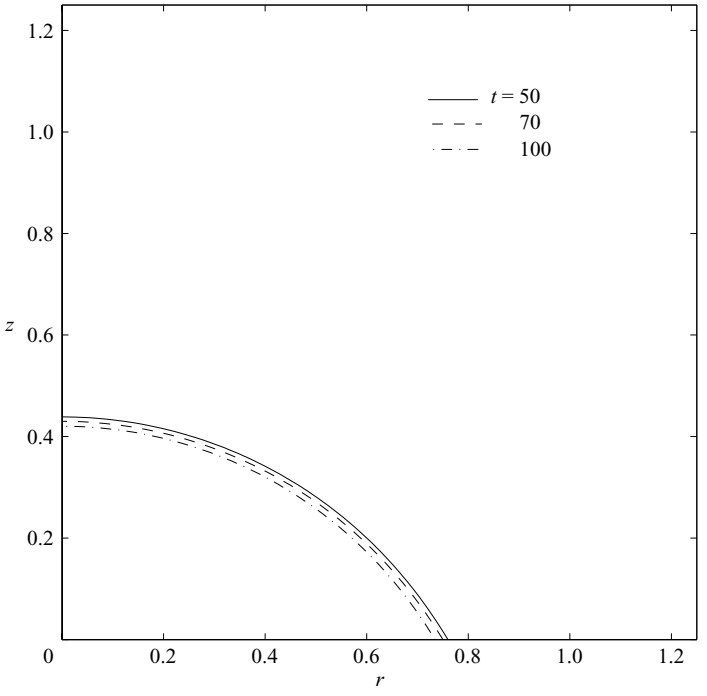

FIGURE 5. Comparison of droplet shapes (for the contour $c = 0$) at various indicated times depicting the solubility inherent in the system. The parameters used in the simulation are the same as those in figure 3.

to $r \propto t^n$ gives $n = 0.24$, 0.3, 0.315 and 0.315 for $\lambda = 0.1$, 1, 10 and 100, respectively. This behaviour is found to hold also for $\theta = 60^\circ$ although with $n = 0.34$.

Foister (1990) reported a similar effect of the viscosity ratio on droplet spreading in the partially wetting regime. It was shown there that the data for different viscosity ratios could be superimposed if Hoffman's correlation H, defined by

$$H = \frac{\cos\theta - \cos\theta_d}{1 + \cos\theta}, \tag{5.1}$$

is plotted against a redefined capillary number, given below:

$$Ca' = \alpha(\lambda)\frac{\eta_d}{\gamma}\frac{\mathrm{d}r_c}{\mathrm{d}t_c} = \alpha(\lambda)\frac{\mathrm{d}r}{\mathrm{d}t}, \tag{5.2}$$

where r_c, t_c and $\mathrm{d}r_c/\mathrm{d}t_c$ represent the dimensional radius of the contact area, time and contact-line speed, respectively. The contact-line speed was obtained by numerical differentiation of the r versus t data. The dynamic contact angle, θ_d in (5.1), was calculated from the drop height and the radius of the contact area using a spherical-cap approximation. The factor α in (5.2) is a shift factor and was found to have a linear dependence on $1/\lambda$ of the form

$$\alpha = \chi\left(1 + \frac{1}{\lambda}\right), \tag{5.3}$$

where χ is a constant. Note that the definition of the viscosity ratio λ used here is the reciprocal of that used in Foister (1990).

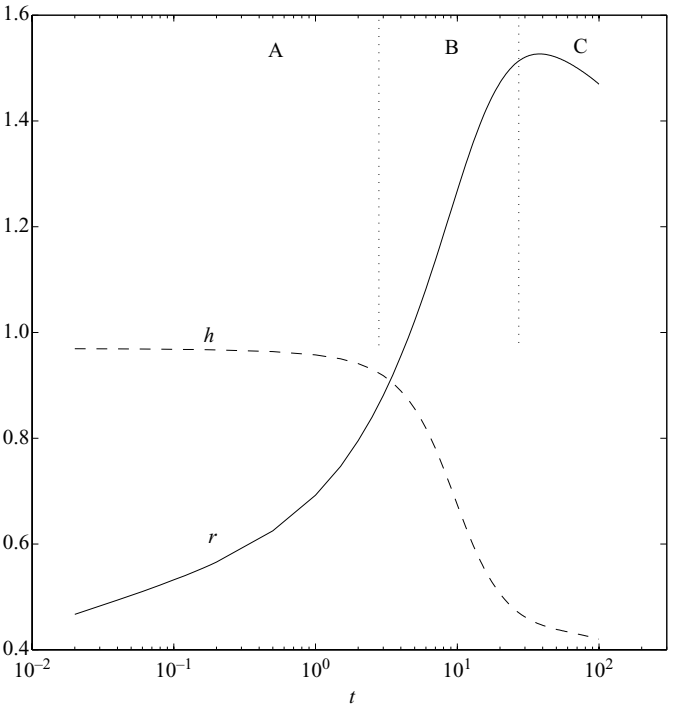

FIGURE 6. Spreading behaviour shown as a plot of r against t. The parameters used in the simulation are the same as those in figure 3. Also, the droplet height h is plotted against t. The three stages observed in the spreading are indicated by A, B and C. Stage A, initial contact angle relaxation; stage B, spreading with a change in the global droplet shape; stage C, spreading halts and/or dissolution occurs.

Our simulation results follow a similar superposition as demonstrated in figures 8 and 9 where Hoffman's correlation H is plotted against the non-dimensional contact-line speed and the redefined capillary number, respectively. The curves are not smooth, owing to the numerical differentiation used to calculate the contact-line speed. On the basis of (5.3), the shift factor α was assumed to have a linear relation with the reciprocal of the viscosity ratio. Using linear regression this relation was found to be

$$\alpha = 1.51\frac{1}{\lambda} + 0.985. \tag{5.4}$$

5.3. *Comparison with the experiments*

Here we compare the diffuse-interface results with the experimental data on droplet spreading in a partially wetting regime reported by Zosel (1993). As a representative case, the spreading behaviour of droplets composed of a PIB solution (in decaline at various PIB concentrations) on a PTFE surface, reported by Zosel (1993), is considered. All the PIB solutions used by Zosel showed nearly the same static contact angles ($\theta \approx 58°$–$60°$) and surface tension. The droplets were 1.2–1.5 mm in radius, and gravity and inertia can be neglected as in the simulations. On a semilogarithmic plot of the dimensionless radius of the contact area against dimensionless time, the results for various PIB solutions were found to be superimposed and to yield a master curve (figure 10). To make the comparison, simulations were performed using the following values for various parameters: $\theta = 56°$, $C_h = 0.02$, $\lambda = 100$, $\Delta t = 5 \times 10^{-3}$ and a mesh

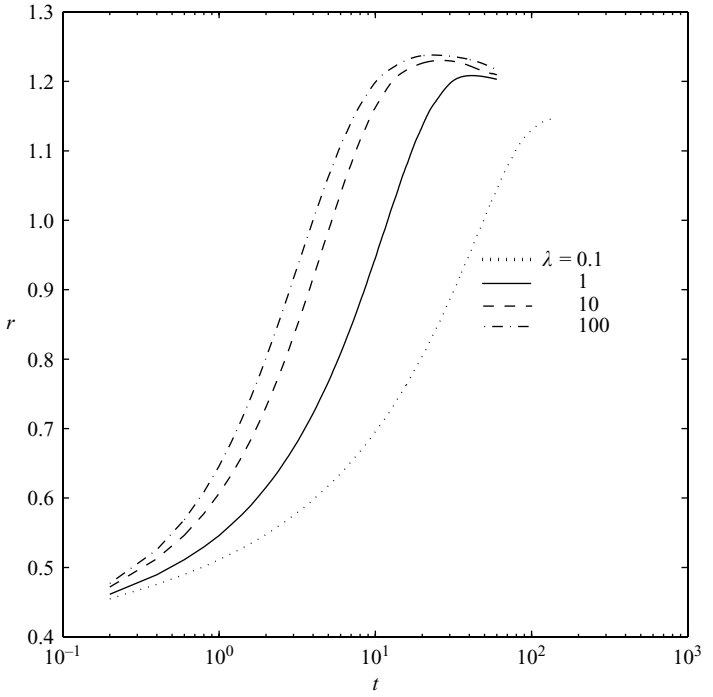

FIGURE 7. Effect of viscosity ratio on the spreading behaviour, for $C_h = 0.02$, $Pe = 50$ and $\theta = 90°$.

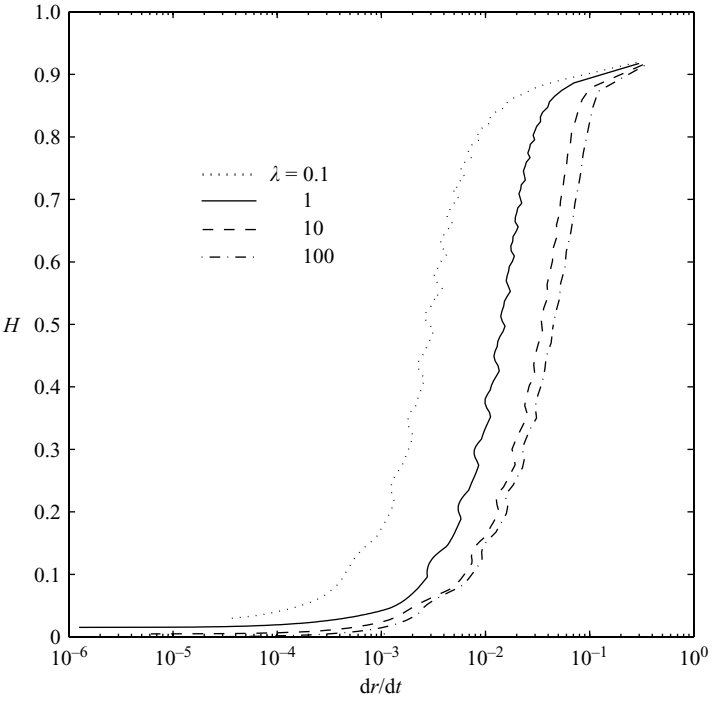

FIGURE 8. Effect of viscosity ratio on the spreading behaviour, plotted as Hoffman's correlation H versus $\mathrm{d}r/\mathrm{d}t$. The parameters used in the simulation are the same as in figure 7.

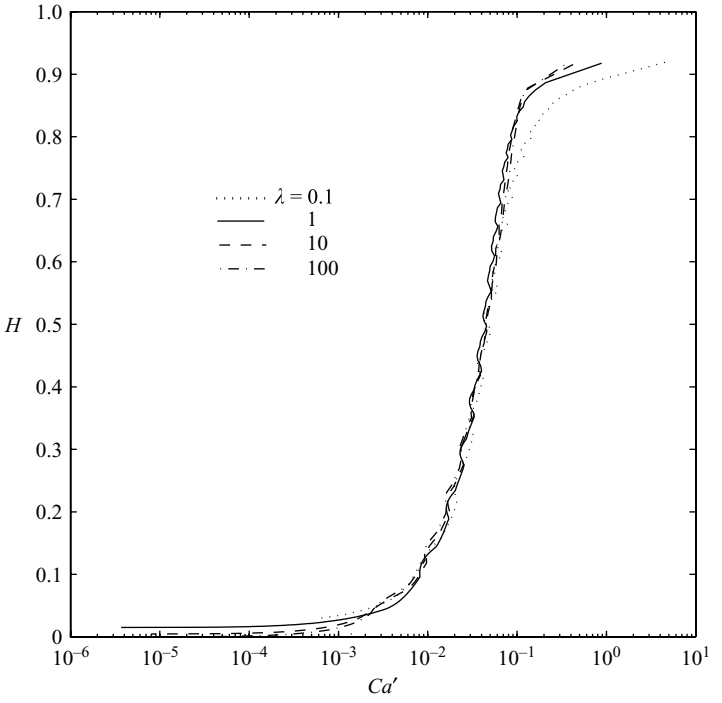

FIGURE 9. Master-curve representation of figure 8 with the data shifted to $\lambda = 100$.

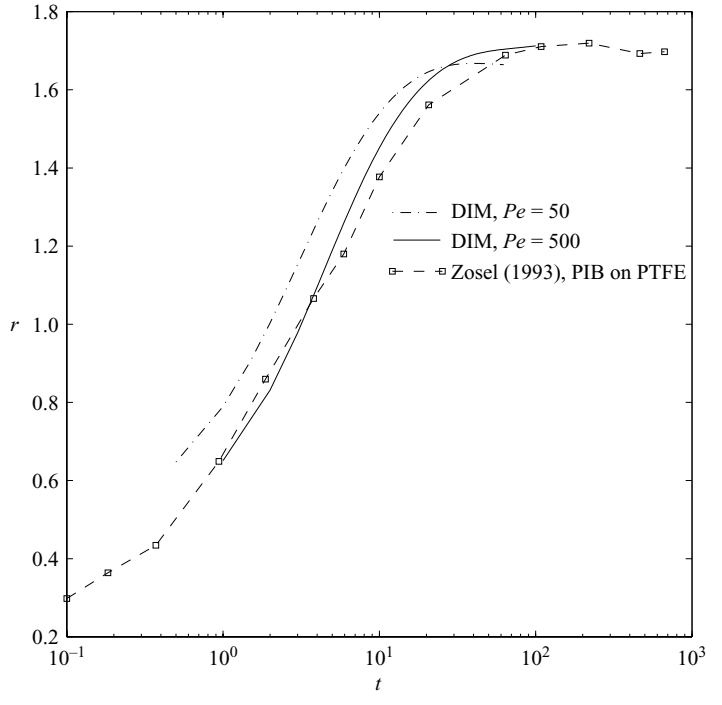

FIGURE 10. Comparison of diffuse-interface spreading behaviour with the experiments of Zosel (1993). The parameters used in the simulation are $C_h = 0.02$, $\lambda = 100$, $\theta = 56°$, $\Delta t = 5 \times 10^{-3}$, with a mesh of 90×90 elements.

of 90×90 elements. In the experiments, λ ranges from 10^3 to 10^6 (for a water droplet in air $\lambda \approx 55$) depending on the concentration of PIB. However, from figure 7, the difference between the spreading behaviour for $\lambda = 100$ and $\lambda = 1000$ is expected to be negligible and hence $\lambda = 100$ is used. The value of C_h is based on numerical convenience and only Pe needed to be assigned a value. First, $Pe = 50$ was used and, as can be seen from figure 10, the diffuse-interface droplet-spreading behaviour is qualitatively similar to that observed experimentally. In fact, when the experimental curve and the one corresponding to $Pe = 50$ are fitted with $r \propto t^n$ for t in the range of 1 to 10, the value of n is found to be identical up to two decimal places for both cases, and equals 0.34. The main difference between the simulation with $Pe = 50$ and the experimental results is in the time scale of the process; DIM leads to faster spreading. Also, the final radius of the contact area obtained from the simulation is smaller than that observed in the experiments. Recalling that Pe is the ratio of convection rate and diffusion rate, the above-mentioned differences indicate that the diffusion rate corresponding to $Pe = 50$ is high. Hence, to improve the quality of the predictions Pe was increased by a factor of 10 to 500. This increase was guided by a rough order-of-magnitude estimate that assumed the droplet diameter, spreading velocity, interface thickness, interfacial tension and mobility to be 10^{-3} m, 10^{-3} m s^{-1}, 1 nm, 70×10^{-3} N m^{-1} and 10^{-17} m^5 s^{-1} J^{-1}, respectively. The droplet diameter of 10^{-3} m roughly represents the maximum diameter for which the influence of gravity can be neglected. The value of mobility used is typical for one liquid diffusing in another in the absence of solids. This value was used since liquid mobilities in the presence of solids are usually not known. The results of the simulation with $Pe = 500$ are also shown in figure 10. Now the simulation and experimental time scales of spreading match and so does the final radius of the contact area. However, the value of n increases from the value found experimentally, 0.34, to 0.37.

5.4. *Effect of wettability*

The effect of substrate wettability is studied by changing the equilibrium contact angle θ using the boundary condition (2.23). First, the calculations were performed for seven different θ values at $Pe = 50$ and $\lambda = 1$. The results are plotted in figure 11. Other than the clearly apparent and expected difference in the final values of r for the seven θ values, the spreading behaviour is seen to be sensitive to the value of the equilibrium contact angle from the very early stages of spreading. Fitting the curves to $r \propto t^n$ for t in between 1 to 10 yields $n = 0.38$, 0.37, 0.35, 0.34, 0.33, 0.3 and 0.215 for $\theta = 20^\circ$, 30°, 45°, 60°, 75°, 90° and 120° respectively. Next, the effect of the wettability on the spreading behaviour was investigated at $Pe = 500$ and $\lambda = 100$, since spreading for these values was found to give good agreement with the experiments of Zosel (1993). The results plotted for five different θ values in figure 12 again show a trend similar to that seen for $Pe = 50$ and $\lambda = 1$, namely, spreading behaviour is sensitive to the value of the equilibrium contact angle from the early stages of spreading. Fitting the curves in figure 12 to $r \propto t^n$ for t in between 1 to 10 now yields $n = 0.395$, 0.38, 0.37, 0.36 and 0.28 for $\theta = 30^\circ$, 45°, 60°, 90° and 120° respectively. This dependence of the spreading behaviour on the equilibrium contact angle is qualitatively similar to the numerical results obtained using a boundary-integral method, as shown by Bazhlekov (2003) and Bazhlekov, Anderson & Meijer (2004) and reproduced here in figure 13. Also, experiments reported by Zosel (1993) where a PAA–water-solution droplet spreads on various substrates showed a similar dependence on the equilibrium contact angle. But this spreading behaviour does not appear to be an universal feature, as demonstrated by a contrasting case where the

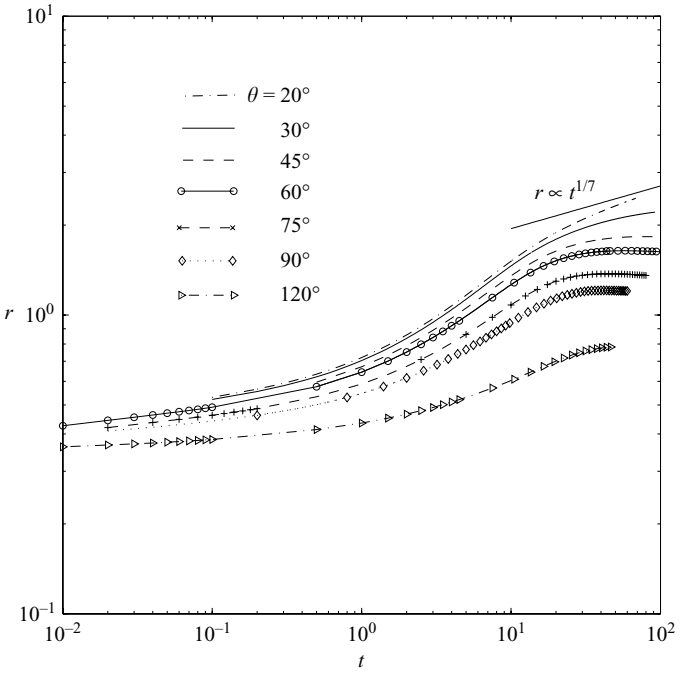

FIGURE 11. Effect of equilibrium contact angle on the spreading behaviour for $C_h = 0.02$, $Pe = 50$ and $\lambda = 1$. The asymptote is added as a guide.

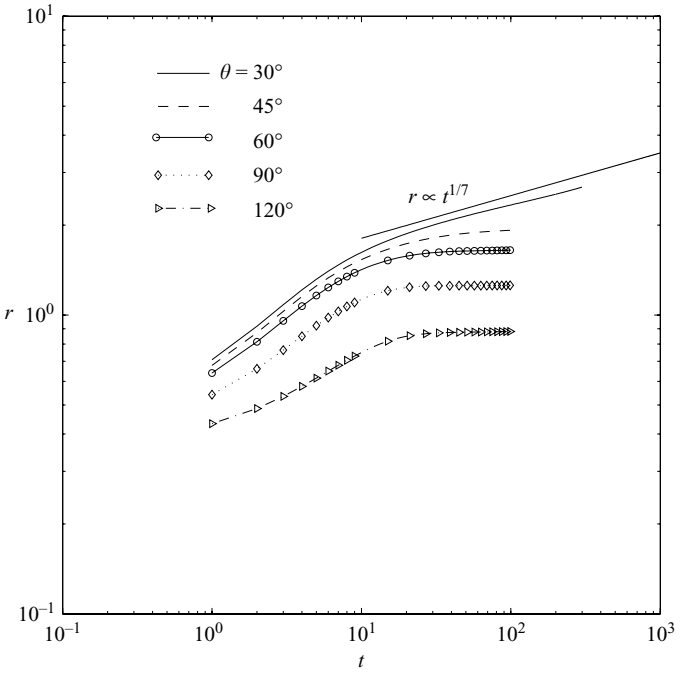

FIGURE 12. Effect of equilibrium contact angle on the spreading behaviour for $C_h = 0.02$, $Pe = 500$ and $\lambda = 100$. The asymptote is added as a guide.

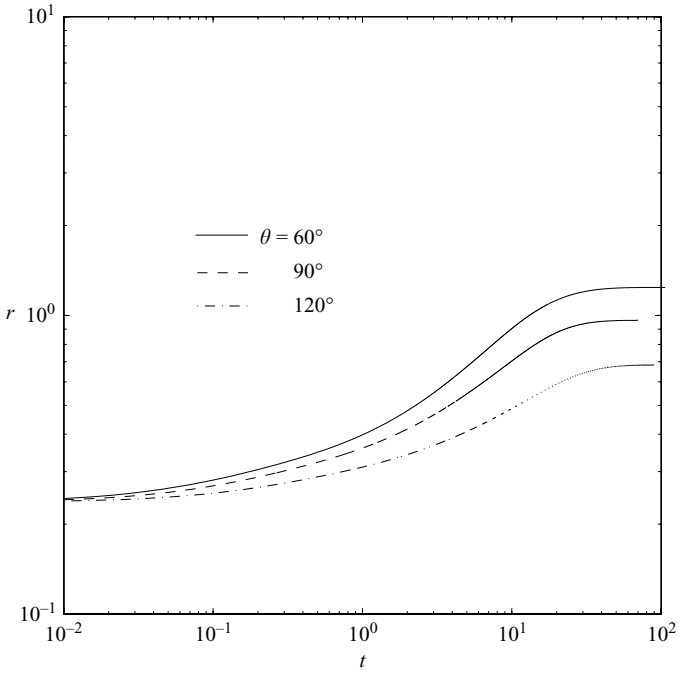

FIGURE 13. Effect of equilibrium contact angle on the spreading behaviour obtained from the boundary-integral method using a slip length of 0.01.

spreading behaviour was found to depend on the equilibrium contact angle only during the last stage of spreading, i.e. for $t > 100$, and to be independent of it before this time, also reported by Zosel (1993). This was found for a droplet of PIB solution in decalin spreading on various substrates (but they were the same as those used for the PAA–water-solution droplet). Although, from the preceding discussion, the dependence of spreading on the equilibrium contact angle from very early stages seems likely to be a universal feature, clearly more experimental data is required to establish it firmly.

For both sets of conditions, i.e. $Pe = 50$ and $\lambda = 1$ and $Pe = 500$ and $\lambda = 100$, the exponent n of $r \propto t^n$ increases with a decrease in θ during the 'short' time range t in between 1 and 10. This increase in n is related to an increase in the driving force for spreading, i.e. the difference between the initially prescribed contact angle of 160° and the equilibrium contact angle. For spreading with $\theta \leqslant 30°$ a second $r \propto t^n$ regime, albeit now with a different n, appears at times $t > 10$; this is better seen in figure 12. The value of n is about 1/5 for $\theta = 20°$, $Pe = 50$ and $\lambda = 1$ while it is 1/8.5 for $\theta = 30°$, $Pe = 500$ and $\lambda = 100$. These values are close to the generally accepted values of 1/7 and 1/10 obtained theoretically and verified experimentally for spreading in the complete wetting regime (see for example Marmur 1983; de Gennes 1985; Dodge 1988; Seaver & Berg 1994). De Gennes *et al.* (1990) and de Ruijter *et al.* (1999, 2000) demonstrated that these values are also valid in the partially wetting regime provided that the equilibrium contact angle is small ($\leqslant 5°$). Owing to computational difficulties associated with simulations of spreading for $\theta < 20°$ we were unable to investigate this point further. However, figures 11 and 12 show that n approaches either of the values known for $\theta = 0°$.

6. Conclusion

Using the diffuse-interface model, droplet spreading in a partially wetting regime was investigated. The diffuse-interface results plotted as the radius of the contact area against time were found to show good agreement with the experimental data of Zosel (1993). The quality of test could be improved by comparing the droplet shapes, instead of just the radius of the contact area, at different times during spreading. The model applied here considered the case of a liquid droplet spreading by displacing ambient liquid. Since inertia can be neglected, the ambient liquid therefore could affect the spreading behaviour only by its viscosity. It was found that the ambient-fluid viscosity affects the time scale of the process but the general spreading behaviour, as shown in the shapes of the r versus t curves, remain the same, and the curves can be superimposed to form a master curve. Finally, the wettability was found to influence the spreading kinetics from the initial stages, which qualitatively matches the predictions from the boundary-integral method.

This work was sponsored by the Dutch Polymer Institute (Project no. 178).

REFERENCES

Amestoy, P. R. & Duff, I. S. 1989*a* Memory management issues in sparse mutlifrontal methods on multiprocessors. *Intl J. Supercomput. Applics.* **7**, 64.

Amestoy, P. R. & Duff, I. S. 1989*b* Vectorization of a multiprocessor mutlifrontal code. *Intl J. Supercomput. Applics.* **3**, 41.

Amestoy, P. R. & Puglisi, C. 2002 An unsymmetrized multifrontal LU factorization. *SIAM J. Matrix Anal. Applics.* **24**, 553.

Anderson, D. M., McFadden, G. B. & Wheeler, A. A. 1998 Diffuse-interface methods in fluid mechanics. *Annu. Rev. Fluid Mech.* **30**, 139–165.

Barrat, J.-L. & Bocquet, L. 1999 Large slip effects at a nonwetting fluid–solid interface. *Phys. Rev. Lett.* **82**, 4671–4674.

Bazhlekov, I. B. 2003 Non-singular boundary-integral method for deformable drops in viscous flows. PhD thesis, Eindhoven University of Technology, the Netherlands.

Bazhlekov, I. B., Anderson, P. D. & Meijer, H. E. H. 2004 Non-singular boundary-integral method for deformable drops in viscous flows. *Phys. Fluids* **16** (4), 1064–1081.

Beveridge, G. S. G. & Schechter, R. S. 1970 *Optimization: Theory and Practice*. McGraw–Hill.

Blake, T. D. 1993 *Dynamic Contact Angles and Wetting Kinetics*, Surfactant Science Series, vol. 49. Marcel Dekker.

Briant, A. J. & Yeomans, J. M. 2004 Lattice Boltzmann simulations of contact line motion. II. Binary fluids. *Phys. Rev.* E **69**, 031603.

Briant, A. J., Wagner, A. J. & Yeomans, J. M. 2004 Lattice Boltzmann simulations of contact line motion. I. Liquid–gas systems. *Phys. Rev.* E **69**, 031602.

Cahn, J. W. 1965 Phase separation by spinodal decomposition in isotropic systems. *J. Chem. Phys.* **42**, 93–99.

Cahn, J. W. 1977 Critical point wetting. *J. Chem. Phys.* **66**, 3667–3672.

Cahn, J. W. & Hilliard, J. E. 1958 Free energy of a nonuniform system. I. Interfacial energy. *J. Chem. Phys.* **28**, 258–267.

Chella, R. & Viñals, J. 1996 Mixing of a two-phase fluid by cavity flow. *Phys. Rev.* E **53**, 3832–3840.

Chen, H.-Y., Jasnow, D. & Viñals, J. 2000 Interface and contact line motion in a two phase fluid under shear flow. *Phys. Rev. Lett.* **85**, 1686–1689.

Cieplak, M., Koplik, J. & Banavar, J. R. 2001 Boundary conditions at fluid–solid interface. *Phys. Rev. Lett.* **86**, 803–806.

Davis, H. T. & Scriven, L. E. 1982 Stress and structure in fluid interfaces. *Adv. Chem. Phys.* **49**, 357–454.

Dodge, F. T. 1988 The spreading of liquid droplets on solid surfaces. *J. Colloid Interface Sci.* **121**, 154–160.

Durbin, P. 1988 Considerations on the moving contact-line singularity, with application to frictional drag on a slender drop. *J. Fluid Mech.* **197**, 157–169.

Dussan V., E. B. 1979 On the spreading of liquids on solid surfaces: static and dynamic contact lines. *Annu. Rev. Fluid Mech.* **11**, 371–400.

Dussan V., E. B. & Davis, S. H. 1974 On the motion of a fluid–fluid interface along a surface . *J. Fluid Mech.* **65**, 71–95.

Foister, R. 1990 The kinetics of displacement wetting in liquid/liquid/solid systems. *J. Colloid Interface Sci.* **136**, 266–282.

Fournier, A., Bunge, H. P., Hollerbach, R. & Villote, J. P. 2004 Application of the spectral-element method to the axisymmetric Navier–Stokes equation. *Geophys. J. Intl* **156**, 682–700.

de Gennes, P. G. 1985 Wetting: statics and dynamics. *Rev. Mod. Phys.* **57**, 827–862.

de Gennes, P. G., Hua, X. & Levinson, P. 1990 Dynamics of wetting: local contact angles. *J. Fluid Mech.* **212**, 55–63.

Gerritsma, M. I. & Phillips, T. N. 2000 Spectral element methods for axisymmetric Stokes problem. *J. Comput. Phys.* **164**, 81–103.

Gunton, J. D., Miguel, M. S. & Sahni, P. S. 1983 *The Dynamics of First-Order Phase Transitions, Phase Transitions and Critical Phenomena*, vol. 8. Academic.

Hocking, L. M. 1977 A moving fluid interface. Part 2. The removal of force singularity by a slip flow. *J. Fluid Mech.* **79**, 209–229.

Huh, C. & Scriven, L. E. 1971 Hydrodynamic model of steady movement of a solid/liquid/fluid contact line. *J. Colloid Interface Sci.* **35**, 85–100.

Jacqmin, D. 1999 Calculation of two-phase Navier–Stokes flows using phase-field modeling. *J. Comput. Phys.* **155**, 96–127.

Jacqmin, D. 2000 Contact-line dynamics of a diffuse fluid interface. *J. Fluid Mech.* **402**, 57–88.

Jasnow, D. & Viñals, J. 1996 Coarse-grained description of thermo-capillary flow. *Phys. Fluids* **8** (3), 660–669.

Joseph, D. D. & Renardy, Y. Y. 1993 *Fundamentals of Two-Fluid Dynamics*. Springer.

Keestra, B., van Puyvelde, P. C. J., Anderson, P. D. & Meijer, H. E. H. 2003 Diffuse interface modeling of the morphology and rheology of immiscible polymer blends. *Phys. Fluids* **15**, 2567–2575.

Kistler, S. F. 1993 *Hydrodynamics of Wetting*, Surfactant Science Series, vol. 49. Marcel Dekker.

Koplik, J., Banavar, J. R. & Willemsen, J. F. 1988 Molecular dynamics of Poiseuille flow and moving contact lines. *Phys. Rev. Lett.* **60**, 1282–1285.

Koplik, J., Banavar, J. R. & Willemsen, J. F. 1989 Molecular dynamics of fluid flow at solid surfaces. *Phys. Fluids* A **1**, 781–794.

Lee, H.-G., Lowengrub, J. S. & Goodman, J. 2002*a* Modeling pinchoff and reconnection in a Hele-Shaw cell. I. The models and their calibration. *Phys. Fluids* **14** (2), 492–513.

Lee, H.-G., Lowengrub, J. S. & Goodman, J. 2002*b* Modeling pinchoff and reconnection in a Hele-Shaw cell. II. Analysis and simulation in the non-linear regime. *Phys. Fluids* **14** (2), 514–545.

Lowengrub, J. & Truskinovsky, L. 1998 Quasi-incompressible Cahn–Hilliard fluids. *Proc. R. Soc. London* A **454**, 2617–2654.

Marmur, A. 1983 Equilibrium and spreading of liquids on solid surfaces. *Adv. Colloid Interface Sci.* **19**, 75–102.

Naumann, E. & He, D. 2001 Nonlinear diffusion and phase separation. *Chem. Engng Sci.* **56**, 1999–2018.

Rowlinson, J. S. & Widom, B. 1989 *Molecular Theory of Capillarity*. Clarendon.

de Ruijter, M. J., Coninck, J. D. & Oshanin, G. 1999 Droplet spreading: partial wetting regime revisited. *Langmuir* **15**, 2209–2216.

de Ruijter, M. J., Charlot, M., Voue, M. & Coninck, J. D. 2000 Experimental evidence of several time scales in droplet spreading. *Langmuir* **16**, 2363–2368.

Seaver, A. E. & Berg, J. C. 1994 Spreading of a droplet on a solid surface. *J. Appl. Polymer Sci.* **52**, 431–435.

Segal, A. 1995 *SEPRAN Manual*. Leidschendam, The Netherlands.

Seppecher, P. 1996 Moving contact lines in the Cahn–Hilliard theory. *Intl J. Engng Sci.* **34**, 977–992.

Shikhmurzaev, Y. D. 1993*a* A two-layer model of an interface between immiscible fluids. *Physica* A **192**, 47–62.

Shikhmurzaev, Y. D. 1993*b* The moving contact lines on a smooth solid surface. *Intl J. Multiphase Flow* **19**, 589–610.

Shikhmurzaev, Y. D. 1994 Mathematical modeling of wetting hydrodynamics. *Fluid Dyn. Res.* **13**, 45–64.

Shikhmurzaev, Y. D. 1997*a* Moving contact lines in liquid/liquid/solid systems. *J. Fluid Mech.* **334**, 211–249.

Shikhmurzaev, Y. D. 1997*b* Spreading of drops on solid surfaces in a quasi-static regime. *Phys. Fluids* **9**, 266–275.

Thompson, P. A. & Robbins, M. O. 1989 Simulations of contact line motion: slip and the dynamic contact angle. *Phys. Rev. Lett.* **63**, 766–769.

Thompson, P. A. & Robbins, M. O. 1990 Shear flow near solids: epitaxial order and flow boundary conditions. *Phys. Rev.* A **41** (12), 6830–6837.

Verschueren, M. 1999 A diffuse-interface model for structure development in flow. PhD thesis, Eindhoven University of Technology, the Netherlands.

Verschueren, M., van de Vosse, F. & Meijer, H. 2001 Diffuse-interface modelling of thermocapillary flow instabilities in a Hele-Shaw cell. *J. Fluid Mech.* **434**, 153–166.

van der Waals, J. D. 1893 The thermodynamic theory of capillarity under the hypothesis of a continuous variation of density. *Verhandel. Konink. Akad. Weten. Amsterdam* **1**. (Engl. transl. by J. S. Rowlinson) in *J. Statist. Phys.* **20** (1979), 197–244.

Yue, P., Feng, J. J., Liu, C. & Shen, J. 2004 A diffuse-interface method for simulating two-phase flows of complex fluids. *J. Fluid Mech.* **515**, 293–317.

Zosel, A. 1993 Studies of the wetting kinetics of liquid drops on solid surfaces. *Colloid Polymer Sci.* **271**, 680–687.